Quantitative Magnetic Susceptibility of the Developing Mouse Brain

by

Ioannis Argyridis

Department of Medical Physics
Duke University

Date:_____

Approved:

_____
Chunlei Liu, Supervisor

_____
Nan-kuei Chen

_____
Robert Reiman

Thesis submitted in partial fulfillment of
the requirements for the degree of
Master of Science in the Department of
Medical Physics in the Graduate School
of Duke University

2012

ABSTRACT

Quantitative Magnetic Susceptibility of the Developing Mouse Brain

by

Ioannis Argyridis

Department of Medical Physics
Duke University

Date:_____

Approved:

_____
Chunlei Liu, Supervisor

_____
Nan-kuei Chen

_____
Robert Reiman

An abstract of a thesis submitted in partial fulfillment of the requirements for the degree of Master of Science in the Department of Medical Physics in the Graduate School of Duke University

2012

Abstract

Cerebral development involves a complex cascade of events which are difficult to visualize in vivo. In this study we combine information from Diffusion Tensor Imaging (DTI) and Quantitative Susceptibility Mapping (QSM) on developing mouse brains at five stages, for three central white matter (WM) regions. QSM can be calculated using frequency-shift Gradient Echo MR images acquired at high-field. Extracted mean values from small white matter regions of QSM brain maps depend on the orientation of the neuronal fibers of each voxel to the main magnetic field B0. Using fiber tracking information from DTI a correlation of the myelin content of regions of interest (ROI) to the orientation of those fibers to B0 can be made. Plots of the myelin anisotropy, as it increases with age, were generated with this method, suggesting that the neuronal axon is paramagnetic while the myelin surrounding the axon is diamagnetic. In addition the fractional anisotropy (FA) and the mean Apparent Diffusion Coefficient (ADC) of the same ROI were plotted against age. Histological exams were also performed to evaluate myelin and iron content. It is confirmed that the main source of magnetic susceptibility in WM is the myelin content. The interpretation of all this brain data will provide valuable information on the architecture of the brain during development and a more accurate diagnosis in the case of a myelin degenerative disease.

Dedication

To my advisor and parents for their guidance and patience.

Contents

List of Figures

Acknowledgements

I would like to thank Dr. Chunlei Liu first and foremost for the opportunity to work with him. He has been an incredible advisor every step of the way. Also I would like to thank Wei Li, post-doc at BIAC, for providing me his Matlab code, presentation figures and expertise every time I needed. Last but not least, I would like thank Luke Xie and Martin Fischer (PhD) of CIVM for helping with the microscope scanning.

1. Introduction

1.1 MRI basics

1.1.1 DTI

Diffusion weighted magnetic resonance imaging (DWI) provides a unique probe into the microstructure of brain tissue by sampling the diffusion properties of water on a microscopic scale much smaller than the macroscopic imaging voxels. The imaging sequence is sensitized to motion on a molecular level by using a bipolar gradient scheme with very high amplitudes, generally referred to as the pulsed gradient spin-echo scheme. Two gradients of same polarity are applied (one before and one after the 180 flip pulse), meaning stationary tissue is equally dephased and rephased. Randomly moving spins however, accrue a net phase loss and appear as a signal loss. Importantly, DWI allows us to probe the properties of water diffusion in various angular directions and hence the diffusion properties of the neuroanatomical environment, which leads to the construction of the Diffusion Tensor (DTI) [40]. This displacement of water, governed by Brownian motion, is highly anisotropic in white matter areas. Traditionally six encoding directions and one with no diffusion weighing are used to reconstruct the tensor. By determining the tensor the true 3D nature of the diffusion process can be realized. It is a rotationally invariant measurement (unlike Apparent Diffusion

Coefficient), i.e., the values are not governed by the orientation of the structure in relation to the magnetic field.

The diffusion tensor is a symmetric 3 × 3 matrix:

$$\vec{D} = \begin{bmatrix} D_{xx} & D_{xy} & D_{xz} \\ D_{yx} & D_{yy} & D_{yz} \\ D_{zx} & D_{zy} & D_{zz} \end{bmatrix}$$

Its diagonal elements (D_{xx} , D_{yy} , D_{zz}) correspond to diffusion along three orthogonal axes. The off-diagonal elements relate diffusion between these axes. When these off-diagonal elements are zero, the tensor is said to be diagonalized in order to obtain three eigenvalues (λ_1 , λ_2 , λ_3)and eigenvectors which describe the diffusion orientation. The eigenvector with the largest eigenvalue represents the preferred or principal direction of diffusion.

1.1.2 Formalin Fixation

After cardiac arrest natural cell degeneration occurs. To prevent this, perfusion fixation with 4% formalin was used. The perfusion fixation procedure uses the cardiac blood flow typically in combination with a pump to flush the fixative through the entire body. The fixative is injected into the heart with the injection volume matching cardiac output and the procedure takes about 5 – 10 min. This has the advantages of preserving perfect morphology because the tissue does (in principle) not start autolysis before fixation [18]. Fixation by immersion into a large volume of fixative gives mixed results in

diffusion studies, since the time delay from cardiac arrest to full immersion impacts the quality of the tissue and MR image. In-vivo imaging is more complicated due to motion artifacts and the iron-containing blood affects susceptibility imaging.

1.1.3 GRE

Gradient Echo, also known as gradient recalled echo, is a type of MR signal created by the application of a gradient reversal. Unlike a spin-echo, it is characterized by the absence of a 180° refocusing pulse leading to shorter repetition times and faster sequences. This also makes the signal inherently T2* weighted and prone to susceptibility artifacts.

As we will see proper signal post-processing of the complex raw k-space rf data, specifically the phase maps can lead to susceptibility weighted imaging (SWI) and quantitative susceptibility mapping (QSM)

1.2 Literature Review

High-field Gradient Echo (GRE) Magnetic Resonance Imaging (MRI) maps show high contrast depending on magnetic susceptibility differences [1]. The source of this contrast is not well understood. Some suggested contrast agents that are naturally present in the brain include: non-heme iron (ferritin), deoxy-hemoglobin (oxygenation) and myelin [2-6]. Thereby this method provides a non-invasive method for mapping such quantities crucial to the functioning and development of the brain.

Magnitude maps have indicated this potential, taking advantage of the fact that relaxation times (R2*) are different in myelin, but they don't have high Contrast to Noise Ratio [7]. Another issue is the macroscopic field gradients due to interfaces between tissue and air. This effect depends on the dimensions of the imaging voxel, increasing with voxel size. Thus, small voxels are preferred, although these can cause signal-to-noise problems especially for highly iron loaded tissues such as liver and the heart [8].

Phase maps have much better CNR [1]. However phase/frequency-shift maps generated from GRE images suffer from artifacts i.e. phase aliasing and the interference of the background low-frequency magnetic field from the air-tissue interface. Several methods are available to reduce phase wrap-around artifacts, such as using spatial saturation bands or phase oversampling methods [10] or using SHARP (Sophisticated Harmonic Artifact Reduction for Phase data) [11] . Also a method exists for the background phase removal that is insensitive to phase aliasing [12].

A conversion between the phase frequency-shift and the magnetic susceptibility exists with a constant phase offset for any given point: $\varphi(\vec{r},T_E) = \varphi_0 - \gamma \Delta B(\vec{r}) T_E$ So by employing two phase maps with two different echo times T_E, Quantitative Susceptibility Maps (QSM) can be reproducibly calculated. Another characteristic of the susceptibility maps is the dependence of values in white matter regions on the orientation of neuronal fibers to the main magnetic field B_0 giving rise to the term magnetic susceptibility

anisotropy [9]. This can be viewed as an artifact that needs to be corrected by taking the mean of maps of brains taken at various angles (multiple orientations) to B_0, thereby providing an advantage over single orientation in SNR but eliminating information about susceptibility anisotropy and is less practical in the clinic [13]. More importantly it can also be viewed as a source of additional information. It is well known from NMR and EPR spectroscopy that bio-molecules and nucleic acids have anisotropic magnetic susceptibility, which can be determined both theoretically and experimentally, and it's used as a molecular/structural identification method [14-15]. Subsequently Liu et al reported that phase maps don't have the usual contrast between gray and white matter in the dysmyelinating shiverer mice where axon structure is intact as demonstrated by diffusion anisotropy but myelin is absent [4,20].

A commonly used way of visualizing the post-natal micro-structural brain changes is water diffusion characteristics of fiber tracts. Macroscopic changes in fiber tracts involving coherence and compaction as well as microscopic changes such as intracellular components and fiber thickness have been extensively documented [16-17]. Diffusion Tensor Imaging (DTI) provides parameters sensitive to these changes: the diagonalized tensor elements λ_1, λ_2 and λ_3 with the first element in the direction of greatest diffusivity as well as the fractional anisotropy (FA) (a measure of how different each element is from the mean) which follow opposite trends. Generally, during brain

maturation mean diffusivity decreases while fractional anisotropy increases. However white matter development is comprised of two opposing biological processes, axonal myelination and pruning. Depending on the timing of peak activity of each process FA might be increasing and then slightly decreasing.

1.3 Aim of this study

The aim of this study is to understand what kind of information QSM can provide in addition to or to complement DTI imaging. We hypothesize that the source of susceptibility anisotropy is most likely to be myelin. Anisotropy of magnetic susceptibility was assessed as a function of age. In addition histological examinations were performed as the gold standard for the detection of iron and myelin.

2 Materials and Methods

Healthy C57BL/6 mice (The Jackson Laboratory, Bar Harbor, ME; Charles River, Raleigh, NC) were anesthetized with Nembutal. To prepare the animal for imaging experiments, a catheter was inserted into the left ventricle of the mouse heart. The animal was perfused with a peristaltic pump with 20 cc of warm (37 °C) 0.9% saline followed by 20 cc of 10% buffered formalin (Buffered Formalde-Fresh; Fisher Scientific) [18]. After perfusion fixation, the heads of the mice were stored in 20% buffered formalin overnight before imaging experiments in the following day. The perfused mouse brain was kept within the skull to prevent any potential damage to the brain caused by surgical removal. The specimen was sealed tightly inside a cylindrical tube (length 30mm and diameter 11mm). The perfusion-fixed mouse brains were scanned on a 9.4 T (400 MHz) 89-mm-diameter vertical bore Oxford magnet with shielded coil providing gradients of 1600 mT/m and a GE EXCITE MR imaging console (GE Healthcare, Waukesha, WI). For the QSM maps the specimens were scanned with a 3D Gradient Echo Sequence (GRE), TE =20ms, TR=200ms, matrix size=368x184x184 and flip angle 40°. For the DTI maps a 3D Spin Echo Sequence was used with parameters: matrix size=165x82x82 with a b-value=1000s/mm^2, TE = 12 ms, TR = 2.5 s. Six encoding directions were used. The encoding directions are (1, 0, 1), (1, 0, −1), (1, 1, 0), (1, −1, 0), (0,

1, 1), and (0, 1, −1). The animal study was approved by the Institutional Animal Care and Use Committee (IACUC) of our institution.

We had 4 brains for each developmental stage (post-natal day 2, 7, 14, 22) and 4 groups giving a total of 16 brains. Additionally a mature brain (day 56) was included. The stages selected represent a time where significant changes occur in infant mouse brain.

The pixel size was adjusted with k-space manipulation to isotropic 60μm for all maps to increase SNR for the QSM maps. Phase data from the GRE were reconstructed, unwrapped and large background phase was removed with the sphere-mean-value filter followed by a deconvolution operation [11] using a 3D-mask, that segments the brain from the skull. The mask was created with ITK-SNAP [19]. The sphere-mean-value filter takes advantage of the harmonic properties of the field -and the induced phase shift- that originates from magnetic susceptibility of homogeneous media outside of the masked region of the brain, using the equation $\nabla^2\varphi = \nabla^2 B = 0$.

Quantitative magnetic susceptibility value was computed for each voxel iteratively using the LSQR algorithm [20] by inverting the following formula: $\Delta f = \gamma\mu_0 H_0 \cdot FT^{-1}\left[\left(\frac{1}{3} - \frac{k_z}{k^2}\right) FT(\chi)\right]$ (eq.1) where Δf is the frequency shift (after unwrapping and background phase removal) and χ is the quantitative and macroscopic magnetic susceptibility, originally proposed by Salomir [21].

Regions-of-interest (ROI) of three white matter structures -Corpus Callosum (CC), Anterior Commissure (AC), and Fornix System (FS) - were manually and conservatively segmented using ITK-SNAP with respect to FA maps.

These regions-of-interest were then scaled onto the QSM maps to match their resolution using Convert3D (part of ITK-SNAP). The weighted average of each ROI and its standard deviation were calculated, giving us quantitative data for the susceptibility, anisotropy and diffusivity of each structure.

Additionally the same brain was scanned with a different angle to the main magnetic field to independently reconstruct susceptibility maps for each orientation (7 to 9 directions per brain). The resulting susceptibility maps were then linearly registered (to the first map of each set) using a transformation matrix with FSL-FLIRT [22] that was computed from registering the magnitude maps of each using ITK-SNAP, thus allowing us to obtain susceptibility measurements of specific regions with a given orientation of the brain to B_0. We also obtained the fiber orientation of each region from the DTI maps, thus allowing us to calculate the dependence of susceptibility on the angle of the fibers to B_0.

Due to the spatial constraints of the solenoid RF coil used to achieve desirable SNR, the brain was only rotated around the anterior-posterior axis. This setup is sufficient to evaluate susceptibility anisotropy but insufficient to evaluate the full

susceptibility tensor as described by Wei Li et al [23] (eq.7) which requires rotation around two axes perpendicular to B_0.

Diffusion tensor images were analyzed as described previously [24]. All the programs were written using Matlab R2010a (Mathworks, Natick, MA). The calculations were performed on the BIAC computational Linux cluster comprised of 61 computing nodes with 8 CPU cores and 32 GB RAM per node, although they can performed on a typical desktop computer as well.[25]

As a gold standard, we performed histological examinations on the same brains. Coronal slices were stained with myelin staining agent (LFB -Luxol Fast Blue) or iron staining agent and then imaged using Axioscop2 FSmot optical microscope with EC Plan-Neofluar Zeiss Lens at 10 x magnification, 0.3 aperture under the same settings and light conditions. Pixel size=1.96μm, 12Bit depth RGB color, resolution=456x344 with 3x3 binning, 5ms exposure time in tile mode. Background shading effects of picture tiling were removed using a blank image with Matlab. Using ImageJ the mean transmitted light intensity of a specific white matter region (external capsule) was assessed with age in contrast to a neighboring gray matter area used as background.

White matter volume estimation was performed on the FA maps by first using a mask created in ITK-SNAP to remove the background and then by thresholding the FA

map. Values above 0.54 are considered as white matter structures. All the FA maps have isotropic 60μm^3 resolution so the number of voxels was converted to volume.

3 Results and Discussion

3.1 Diffusion results

See figures on the next page.

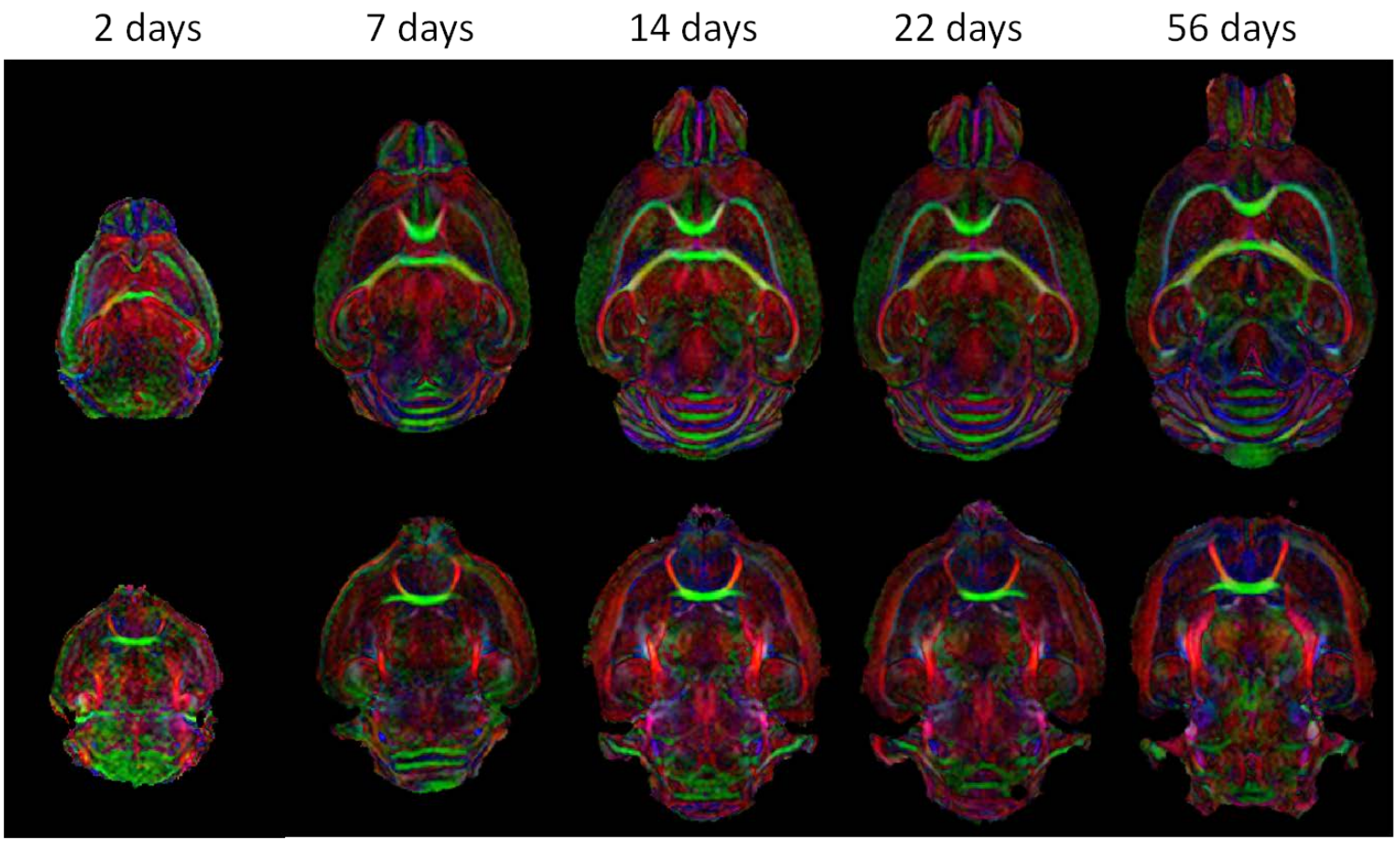

Figure 1: Diffusion Tensor Imaging with color-coded eigenvectors of the developing mouse brain.

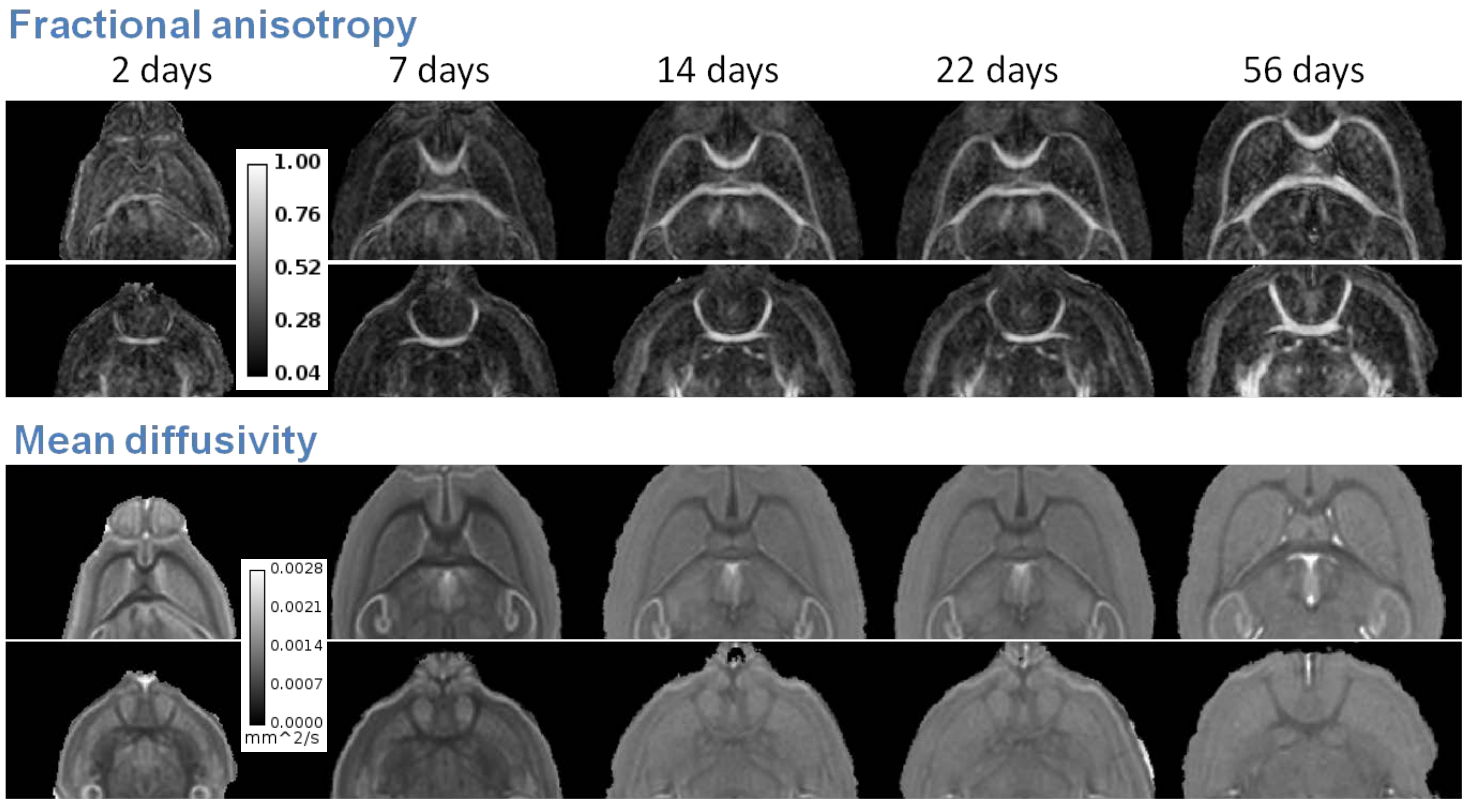

Figure 2: Fractional Anisotropy and Mean Diffusivity Maps of the developing mouse brain. The high contrast of white matter structure in FA maps makes them ideal for manual ROI selection. Subsequently the coordinates are transformed to QSM to obtain exactly the same structures.

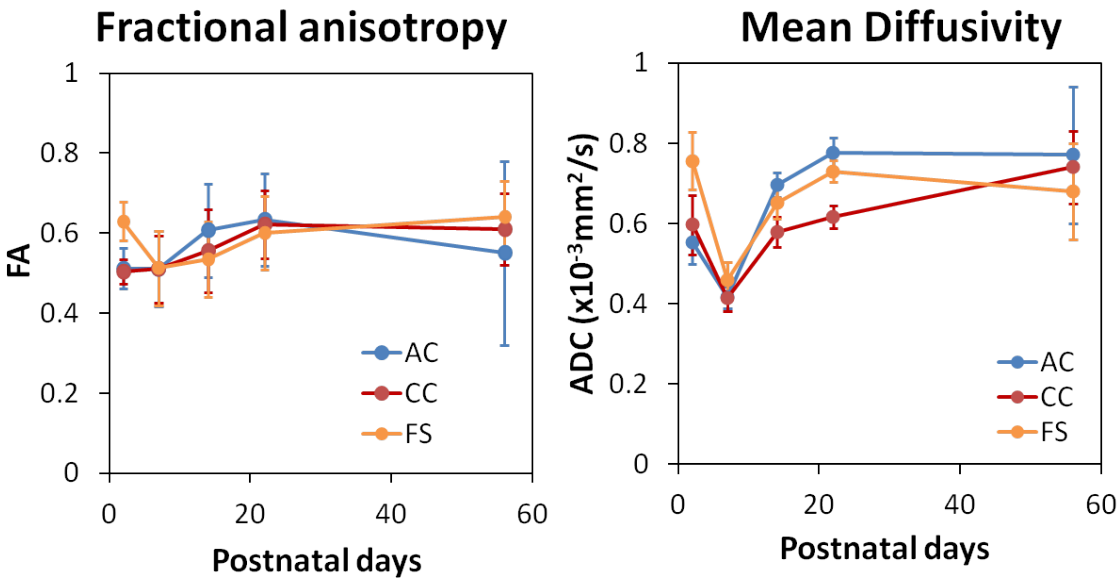

Figure 3: extracted values of FA and ADC from white matter regions-of-interest as a function of age. Anterior Commissure (AC), Corpus Callosum (CC), Fornix System (FS)

The changes in FA agree with previous findings [27] that show an increase from 0.4 to 0.6 for CC and AC. The small drop in FA for FS could be due to PVE (partial volume effects) and the concurring FA drop in surrounding gray matter during the first post-natal week. However the lower diffusivity that occurs only at day 7 is inconsistent with previous findings. Such inconsistencies may arise from differences between samples in formalin fixation. During white matter maturation diffusivity usually decreases and anisotropy increases.

It is suggested that in-vivo measurements of DTI may reflect more accurately normal physiological conditions although several practical issues arise in that scenario such as brain motion and the need for repeated scans to obtain high SNR. [2]

In vivo DTI of rat brains was studied by [29] suggesting that the rise in FA and decrease in diffusivity values for the CC may be attributed to axonal pruning and/or apoptosis during the same developmental period.

A closer look on DTI metrics in live mice that uses axial and radial diffusivities instead of mean ADC shows that both of these values reach a peak around day 12 [30], giving the FA a small dip around day 12. The values of FA and the shape of the plot are in agreement with Fig.3.

DTI has been used to detect demyelination and evaluate recovery in mice [31] but as noted [16] many factors influence DTI metrics including myelin and axonal membrane thickness, reduction in brain water, axonal packing. Furthermore myelination continues on after anisotropy has leveled off. Although it is clinically helpful to link changes in DTI solely to myelination during development, the evidence in the literature indicates that it would certainly be an oversimplification. And this limitation of DTI is supported by our data. As shown in Fig. 1, diffusion anisotropy did not show significant visual difference among different ages, although it is clear that the brains were not well myelinated in first three weeks of age.

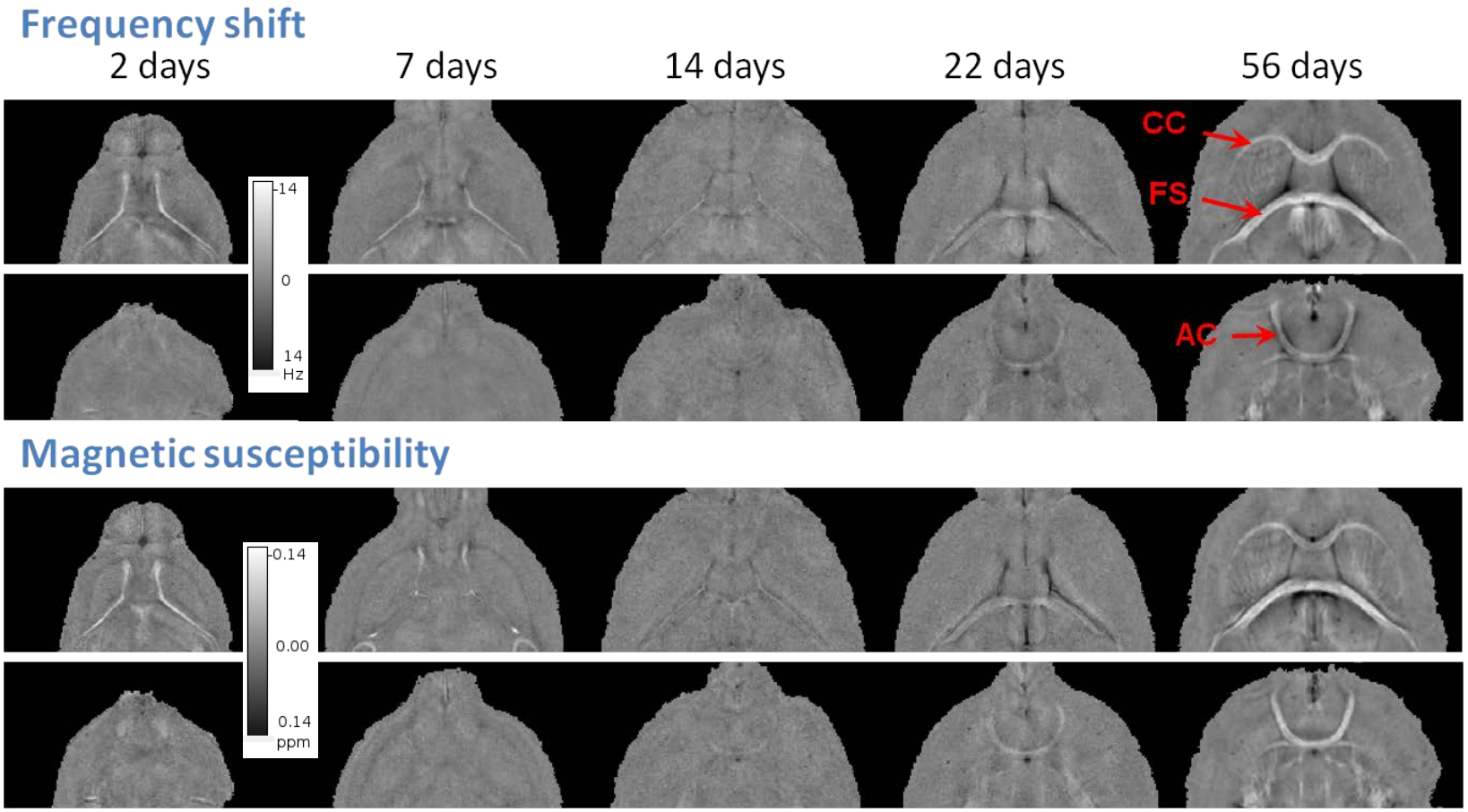

Figure 4: Frequency Shift and Magnetic Susceptibility maps. Arrows point at white matter regions-of-interest.

3.2 Susceptibility results

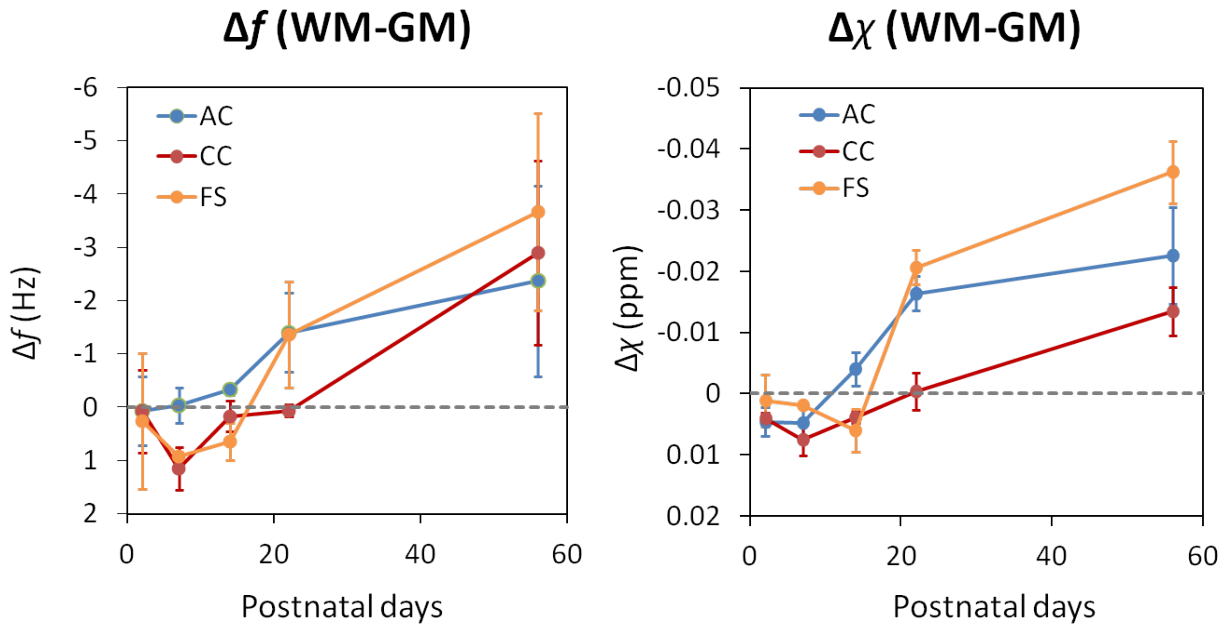

Figure 5: Frequency shift contrast (left) and Magnetic Susceptibility contrast (right) of selected white matter regions to neighboring gray matter regions as a function of age.

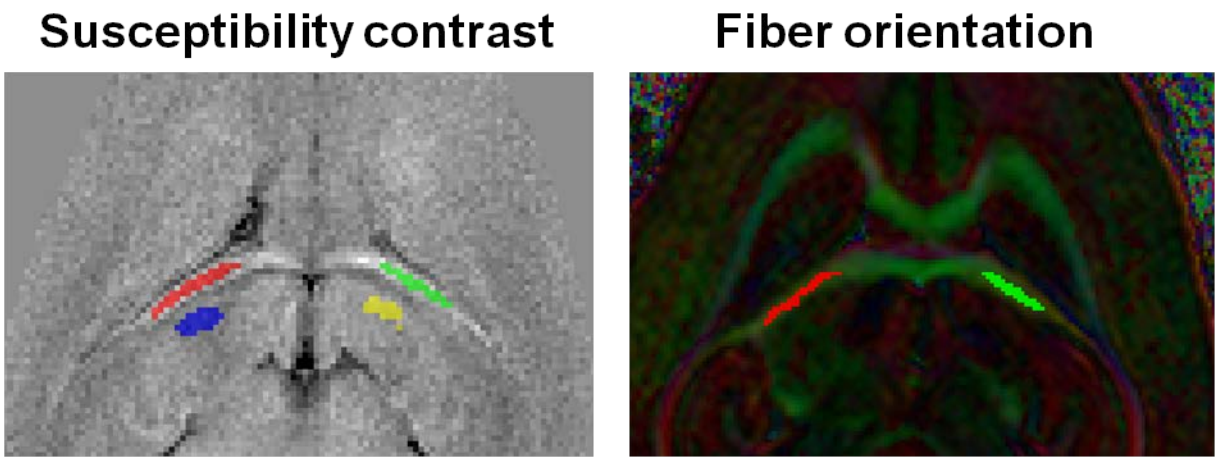

Figure 6: Manual ROI selection of neighboring gray matter for contrast calculations on magnetic susceptibility maps (left) and manual ROI selection on color-coded diffusion maps for fiber bundle orientation of the same ROI (right).

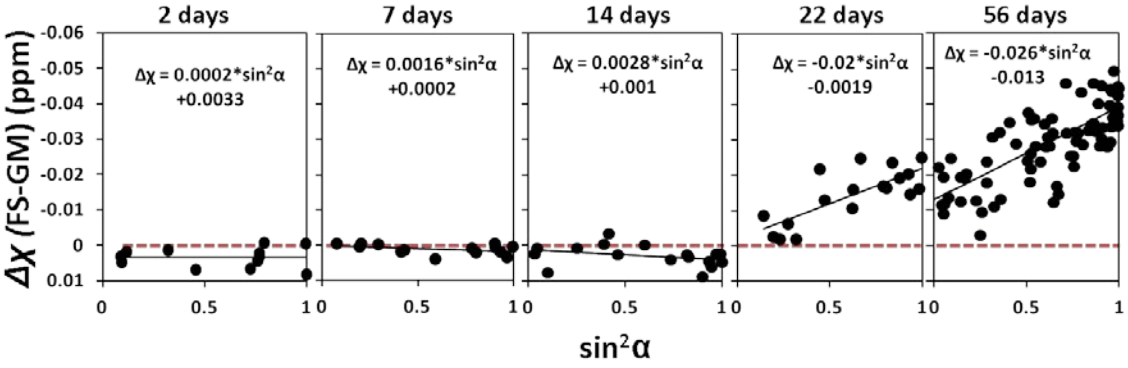

Figure 7: orientation dependence of the QSM to the angle α between the main magnetic field and the main neuronal axons in a specific ROI. The difference of the susceptibility of the fornix system to that of a nearby gray matter region was plotted as function of $\sin^2(\alpha)$. We observe an increase in the slope of the fitted trend line as we progress through days.

Fig. 5 shows the major changes in myelination that can be detected through frequency-shift and susceptibility differences in prominent white matter structures. As expected, gray matter and unmyelinated white matter are paramagnetic in the early days. During the course of the first 4 weeks this changes dramatically, as we can see when myelin begins to form around the neurons in white matter. Myelin, acting as an insulator, is diamagnetic, thus the higher contrast observed in Fig. 4 during development. The quantitative comparison displayed in Fig. 5 allows us to notice different rates of myelination for different structures. Furthermore the point of zero frequency-shift or susceptibility difference, meaning zero contrast in the maps, depends upon the structure under consideration as well.

In the previous quantitative comparison the brains were positioned in the same way in the scanner for each developmental stage. Fig. 6 provides a new kind of information, by combining extracted values from QSM and DTI maps in each of the 5 graphs corresponding to the 5 age groups. We scanned each brain repeatedly, rotating it in the bore after each scan, giving us 7-9 susceptibility maps per age group. From these maps we extract the difference of the susceptibility of the fornix system to that of nearby gray matter. The orientation of the neuronal fibers relative to the B_0 at each point is known since the maps are registered to each other and to the DTI map containing the principal diffusion eigenvectors. Finally that difference of the susceptibility is plotted against the $\sin^2(\alpha)$, where α is the angle of the orientation of the neuronal fibers to B_0.

During the first 4 weeks in mouse brains myelin begins to form around the axons. Myelin at the molecular level, as most biomolecules, is known to have anisotropic magnetic susceptibility which is used to determine structure in NMR and EPR spectroscopy [34]. For MRI, the ordered arrangement of myelin lipids results in a macroscopic magnetic susceptibility anisotropy. This is accomplished by the pattern of the phospholipid bilayers in myelin that align in a cylindrical structure around the axon nerve during maturation and enable us to observe the increase in anisotropy as it is represented by the increase of the slope in the successive graphs of Fig.7 during development. However myelin is not the only longitudinally oriented structure. Other structures like the axonal membrane and the neurofibrils (microtubules,

neurofilaments), which still exist in the shiverer mouse, provide structural support, nutrition and reduce water diffusion radially but their magnetic properties are similar to that of the axons in the background, hence they don't create contrast in QSM [33]. On the other hand, iron-carrying molecules such as tissue iron and deoxy-hemoglobin have strong paramagnetic properties but lack spatial coherence. As we can see from the iron stained histological samples in Fig.8 iron is present and spread almost evenly from the early post natal days but does not create considerable contrast in QSM. In short myelin lipids appear to be the main source of macroscopic susceptibility anisotropy. According to [23] the formula depicted is: $\chi = f_{lipid}\left(\frac{\chi^{axon\perp B_0} - \chi^{axon // B_0}}{2}\right)\sin^2\alpha + \chi_0$ where f_{lipid} is the volume fraction of myelin lipids, χ_0 is the baseline susceptibility due to choice of frame of reference and isotropic susceptibility effects.

3.2 Staining results

Of critical value to test our hypothesis that QSM depends on myelin (and possibly other proteins that are associated with the production of myelin) is the explanation of the dip that we observe in susceptibility on day 7 in Fig.5, which could be due to iron (iron is 61-88% in the form of ferritin and is super-paramagnetic [35]) accumulation which is taken up by oligodendrocytes to produce myelin.

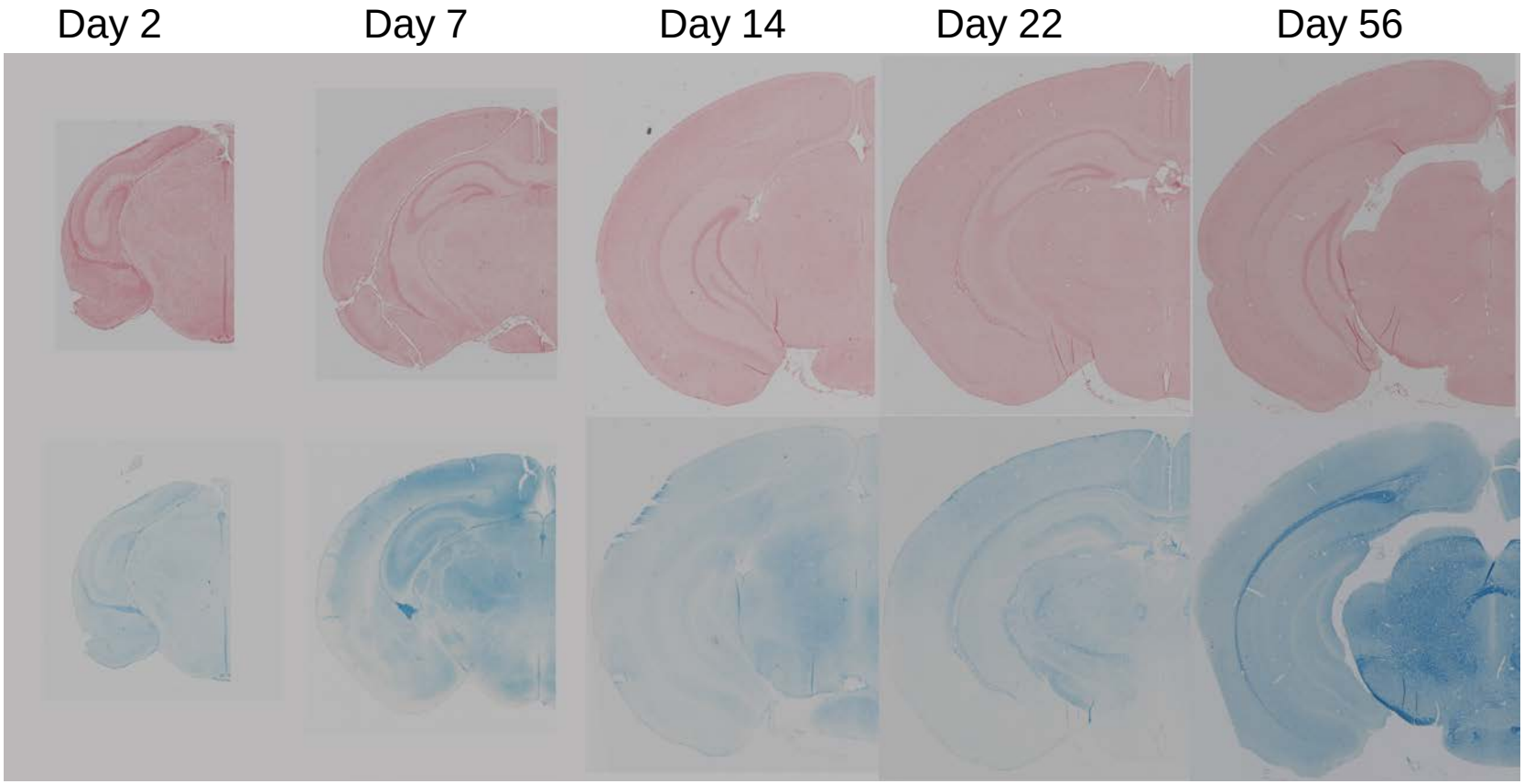

Figure 8: 2µm ferritin(above) and myelin(below) stained coronal slices under light microscopy

In particular H-ferritin stimulates development of oligodendrocyte progenitor cells (OPCs) by increasing expression of myelin basic protein (MBP) [36]. In Fig.9 of iron contrast in the stained microscope slices we observe a maximum around day 7 followed by a minimum on day 14 of iron content relative to the gray matter background. This could be explained with the maturation timings of the different white matter structures.

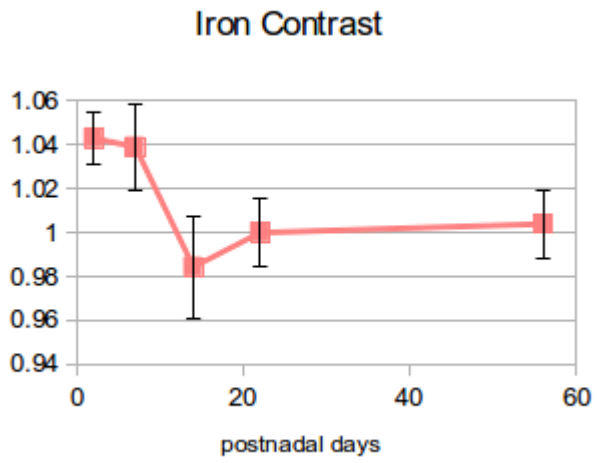

Figure 9: Iron contrast of the external capsule to neighboring gray matter structure as a function of age from 2μm coronal ferritin stained slices.

The increase of myelin in coronal slices as depicted by LFB staining in Fig.10 agrees well with the decrease in susceptibility we see in Fig.5. To demonstrate this, a correlation figure of iron or myelin contrast to susceptibility contrast is shown in Fig.11 for the Corpus Callosum (including the external capsule). We observe poor correlation between iron and susceptibility but high correlation between myelin and susceptibility.

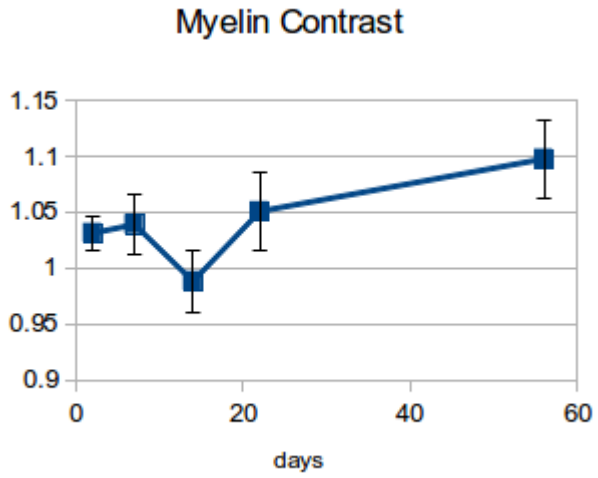

Figure 10: Myelin contrast of the external capsule to neighboring gray matter structure as a function of age from 2μm coronal ferritin stained slices.

For Fig.10, the dip we see around day 14 depending on the maturation timing of white matter structure could be iron accumulation, as previously suggested. Another possible explanation is water content of white matter as it expands during maturation. Rapid volume increase, possibly by water absorption, could lead to a change of the average susceptibility used in the calculations as a reference for each susceptibility map. To this end the following Fig.12 was generated. It shows a rapid white matter volume increase from day 7 to day 14, as it was estimated by thresholding fractional anisotropy maps.

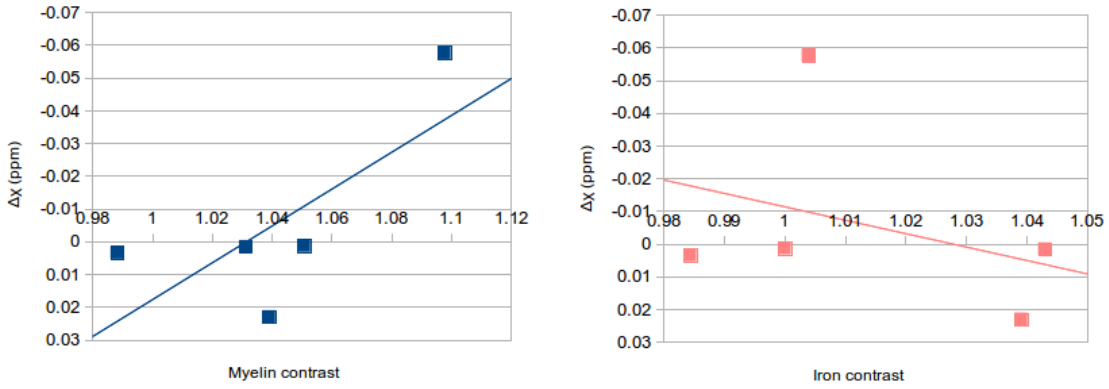

Figure 11: Correlation of myelin or iron contrast to susceptibility contrast for the corpus callosum (including the external capsule).

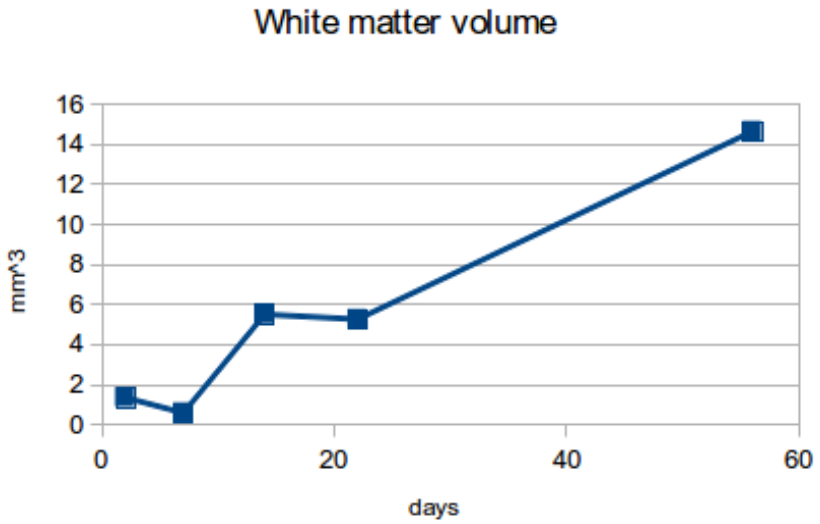

Figure 12: White matter volume measurement estimated by thresholding of FA maps.

It has been suggested that the cerebrospinal fluid or formalin in the ventricles could be used as internal reference in the diffusion maps. To this end the following Fig.13 was generated showing that for at least the first 22 days we have almost constant mean diffusivity. However the increase at day 56 is considerable so normalization

factors from Fig.13 are used to calibrate Fig.3 and the result can be seen in Fig.14. The ADC has a general decreasing trend as it's expected.

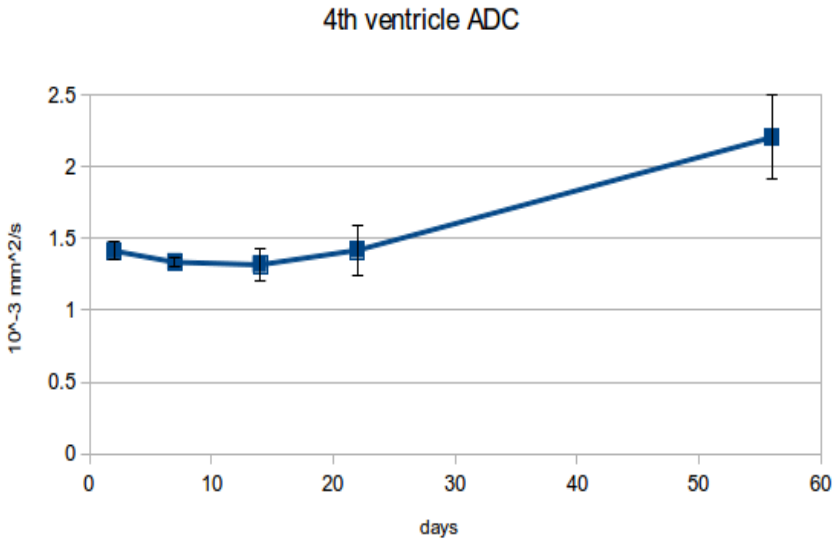

Figure 13: It has been suggested that the CSF/formalin in the ventricles remains of constant diffusivity throughout development if the b-value remains the same for all scans. Here we measure the ADC of the 4th ventricle to verify that.

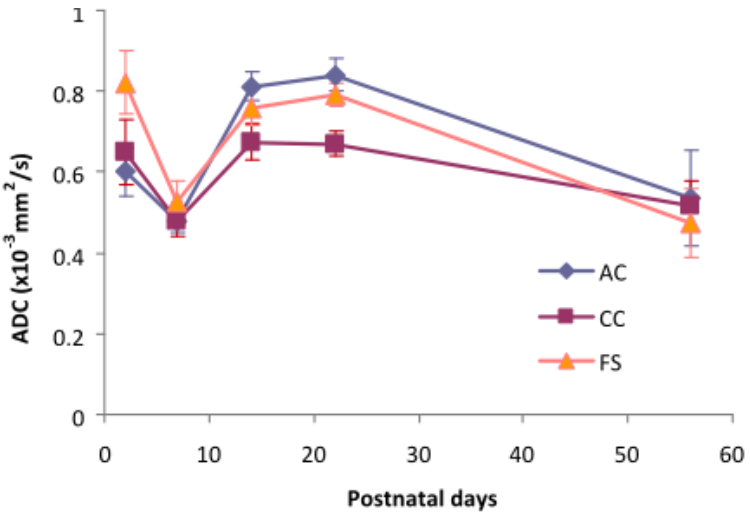

Figure 14: Normalizations factors computed from Fig. 13 are used to calibrate Fig.3. The ADC now has a decreasing trend.

A review of other methods to assess myelin shows the advantages of our method. MTR (Magnetization Transfer Ratio), which is directly proportional to the density of myelin in white matter, is shown to be strongly and linearly correlated to frequency-shift. [32].The same study shows that R2* correlates well with both myelin and iron concentrations. The advantage of frequency resonance shift over R2* is that it can differentiate between iron (paramagnetic) and myelin (diamagnetic) since they have opposing effects and shift the frequency in opposite direction. A step further is the advantage of QSM over frequency-shift. As demonstrated by Liu et al [33] raw phase maps contain severe artifacts from wrap around and background phase, which can be removed before applying eq.1. In addition susceptibility is an inherent property of the tissue under consideration and its quantification is more valuable as it is not affected by arbitrary user-defined scanner settings and the long range dipole effects that may contaminate adjacent structures with different frequency shift.

A comparative study between shiverer mice, that lack myelin, and a normal control group further strengthens the claim that susceptibility differences between gray and white matter are induced by myelin content [33].

Despite our best efforts, several challenges need to be addressed: Diffusion in-vitro is highly perturbed by formalin fixation, but in moving to in-vivo imaging iron blood levels interfere with susceptibility. Susceptibility measurements are not absolutely quantitative since phase unwrapping is imperfect and water used as the reference to

which susceptibility is measured is slightly diamagnetic and changing in density and volume during development. Additionally the linear relation between phase and echo time may not hold true in case of non-laminar flow artifacts, high noise level or partial volume effects.

LFB and Ferritin staining, although common, is also not absolutely quantitative due to shadowing effects and staining agent density/fixation time variations. Other quantitative methods to measure myelin and iron concentrations include PIXE (Particle Induced X-ray Emission) [36] and Synchroton X-ray Fluoresence Iron Mapping [12]. These methods may allow the testing of proposed models of the relative contribution of iron and myelin but only post-mortem.

Future prospects include automation of the process (ROI selection using automatic atlas-based image segmentation) and possibly including an object of known susceptibility in the scanner FOV for reference purposes. Once reliability and replication of results is confirmed in-vivo applications of QSM would be very useful clinically. Apart from visualizing normal brain structures during development with conspicuity, other clinical applications of QSM include the detection of lesions of various pathologic conditions and aids in characterizing tumors and degenerative diseases of the brain [37].

Work recently done by Lodygensky et al [38] verifies our claim that susceptibility maps allow local assessment of myelination during development or disease. Further

work to understand how myelin affects the gradient echo signal is an essential step toward fully understanding WM contrast [39].

4. Conclusion

Diffusivity imaging in vitro, although affected by fixation, still provides reliable and useful white matter anatomic information.

Furthermore, it is possible to conclude that although there are other organized structures that influence QSM, myelin has the dominant role. QSM provides information about the white matter maturation process previously unattainable.

Therefore, magnetic resonance phase imaging based on the proposed contrast mechanism that calculates susceptibility from phase maps, could potentially be applied for in vivo studies of pathologies on a macromolecular level to assess myelin content.

References

[1] J. H. Duyn, P. van Gelderen, T.-Q. Li, J. a de Zwart, A. P. Koretsky, and M. Fukunaga, "High-field MRI of brain cortical substructure based on signal phase.," Proceedings of the National Academy of Sciences of the United States of America, vol. 104, no. 28, pp. 11796–801, Jul. 2007.

[2] K. Shmueli, J. a de Zwart, P. van Gelderen, T.-Q. Li, S. J. Dodd, and J. H. Duyn, "Magnetic susceptibility mapping of brain tissue in vivo using MRI phase data.," Magnetic resonance in medicine: official journal of the Society of Magnetic Resonance in Medicine / Society of Magnetic Resonance in Medicine, vol. 62, no. 6, pp. 1510–22, Dec. 2009.

[3] E. M. Haacke, N. Y. C. Cheng, M. J. House, Q. Liu, J. Neelavalli, R. J. Ogg, A. Khan, M. Ayaz, W. Kirsch, and A. Obenaus, "Imaging iron stores in the brain using magnetic resonance imaging.," Magnetic resonance imaging, vol. 23, no. 1, pp. 1–25, Jan. 2005.

[4] C. Liu, W. Li, B. Wu, Y. Jiang, and G. A. Johnson, "3D fiber tractography with susceptibility tensor imaging.," NeuroImage, vol. 59, no. 2, pp. 1290–8, Jan. 2012.

[5] H. Lu and Y. Ge, "Quantitative evaluation of oxygenation in venous vessels using T2-Relaxation-Under-Spin-Tagging MRI.," Magnetic resonance in medicine◎: official journal of the Society of Magnetic Resonance in Medicine / Society of Magnetic Resonance in Medicine, vol. 60, no. 2, pp. 357–63, Aug. 2008.

[6] X. Li, D. S. Vikram, I. A. L. Lim, C. K. Jones, J. a D. Farrell, and P. C. M. van Zijl, "Mapping magnetic susceptibility anisotropies of white matter in vivo in the human brain at 7 T.," NeuroImage, vol. 62, no. 1, pp. 314–30, Aug. 2012.

[7] A. MacKay, K. Whittall, J. Adler, D. Li, D. Paty, and D. Graeb, "In vivo visualization of myelin water in brain by magnetic resonance.," Magnetic resonance in medicine◎: official journal of the Society of Magnetic Resonance in Medicine / Society of Magnetic Resonance in Medicine, vol. 31, no. 6, pp. 673–7, Jun. 1994.

[8] J. C. Wood and N. Ghugre, "Magnetic resonance imaging assessment of excess iron in thalassemia, sickle cell disease and other iron overload diseases.," Hemoglobin, vol. 32, no. 1–2, pp. 85–96, Jan. 2008.

[9] Lee, J., Shmueli, K., Fukunaga, M., van Gelderen, P., Merkle, H., Silva, A. C., & Duyn, J. H. (2010). "Sensitivity of MRI resonance frequency to the orientation of brain

tissue microstructure.," *Proceedings of the National Academy of Sciences*, *107*(11), 5130-5135.

[10] A. Stadler, W. Schima, A. Ba-Ssalamah, J. Kettenbach, and E. Eisenhuber, "Artifacts in body MR imaging: their appearance and how to eliminate them.," *European radiology*, vol. 17, no. 5, pp. 1242–55, May 2007.

[11] F. Schweser and B. Lehr, "A novel approach for separation of background phase in SWI phase data utilizing the harmonic function mean value property," *Stockholm, Sweden: …*, vol. 18, p. 2010, 2010.

[12] F. Schweser, A. Deistung, B. W. Lehr, and J. R. Reichenbach, "Quantitative imaging of intrinsic magnetic tissue properties using MRI signal phase: An approach to in vivo brain iron metabolism?," *NeuroImage*, vol. 54, no. 4, pp. 2789–2807, Oct. 2010.

[13] S. Wharton and R. Bowtell, "Whole-brain susceptibility mapping at high field: a comparison of multiple- and single-orientation methods.," *NeuroImage*, vol. 53, no. 2, pp. 515–25, Nov. 2010.

[14] Prestegard, "NMR supplement New techniques in structural NMR — anisotropic interactions," *Nature*, vol. 391, no. july, pp. 517–522, 1998.

[15] D. L. Bryce, "Experimental and Theoretical Determination of Nucleic Acid Magnetic Susceptibility: Importance for the Study of Dynamics by Field-Induced Residual Dipolar Couplings," no. Table 2, pp. 10820–10821, 2004.

[16] C. Beaulieu, "The basis of anisotropic water diffusion in the nervous system - a technical review.," *NMR in biomedicine*, vol. 15, no. 7–8, pp. 435–55, 2002.

[17] J. Neil, J. Miller, P. Mukherjee, and P. S. Hüppi, "Diffusion tensor imaging of normal and injured developing human brain - a technical review.," *NMR in biomedicine*, vol. 15, no. 7–8, pp. 543–52, 2002.

[18] Johnson, G. A., Cofer, G. P., Gewalt, S. L., & Hedlund, L. W. (2002). Morphologic Phenotyping with MR Microscopy: The Visible Mouse1. *Radiology*, *222*(3), 789-793.

[19] P. a Yushkevich, J. Piven, H. C. Hazlett, R. G. Smith, S. Ho, J. C. Gee, and G. Gerig, "User-guided 3D active contour segmentation of anatomical structures: significantly improved efficiency and reliability.," *NeuroImage*, vol. 31, no. 3, pp. 1116–28, Jul. 2006.

[20] C. Liu, "Susceptibility tensor imaging.," *Magnetic resonance in medicine: official journal of the Society of Magnetic Resonance in Medicine / Society of Magnetic Resonance in Medicine*, vol. 63, no. 6, pp. 1471–7, Jun. 2010.

[21] R. Salomir, B. D. de Senneville, and C. T. Moonen, "A fast calculation method for magnetic field inhomogeneity due to an arbitrary distribution of bulk susceptibility," *Concepts in Magnetic Resonance*, vol. 19B, no. 1, pp. 26–34, Oct. 2003.

[22] M. Jenkinson, P. Bannister, M. Brady, and S. Smith, "Improved Optimization for the Robust and Accurate Linear Registration and Motion Correction of Brain Images," *NeuroImage*, vol. 17, no. 2, pp. 825–841, Oct. 2002.

[23] W. Li, B. Wu, A. V. Avram, and C. Liu, "Magnetic susceptibility anisotropy of human brain in vivo and its molecular underpinnings.," *NeuroImage*, vol. 59, no. 3, pp. 2088–97, Feb. 2012.

[24] P. J. Basser and C. Pierpaoli, "Microstructural and physiological features of tissues elucidated by quantitative-diffusion-tensor MRI.," *Journal of magnetic resonance. Series B*, vol. 111, no. 3, pp. 209–19, Jun. 1996.

[25] W. Li, B. Wu, and C. Liu, "Quantitative susceptibility mapping of human brain reflects spatial variation in tissue composition.," *NeuroImage*, vol. 55, no. 4, pp. 1645–56, Apr. 2011.

[26] D. J. Pinero and J. R. Connor, "Iron in the Brain: An Important Contributor in Normal and Diseased States," *The Neuroscientist*, vol. 6, no. 6, pp. 435–453, Dec. 2000.

[27] S. Baloch, R. Verma, H. Huang, P. Khurd, S. Clark, P. Yarowsky, T. Abel, S. Mori, and C. Davatzikos, "Quantification of brain maturation and growth patterns in C57BL/6J mice via computational neuroanatomy of diffusion tensor images.," *Cerebral cortex (New York, N.Y.◎ : 1991)*, vol. 19, no. 3, pp. 675–87, Mar. 2009.

[28] H. Chahboune, L. R. Ment, W. B. Stewart, X. Ma, and D. L. Rothman, "Neurodevelopment of C57B / L6 mouse brain assessed by in vivo diffusion tensor imaging," *NMR in Biomedicine*, pp. 375–382, 2007.

[29] K. H. Bockhorst, P. a Narayana, R. Liu, P. Ahobila-Vijjula, J. Ramu, M. Kamel, J. Wosik, T. Bockhorst, K. Hahn, K. M. Hasan, and J. R. Perez-Polo, "Early postnatal development of rat brain: in vivo diffusion tensor imaging.," *Journal of neuroscience research*, vol. 86, no. 7, pp. 1520–8, May 2008.

[30] P. Larvaron, O. Boespflug-tanguy, J. Renou, and J. Bonny, "In vivo analysis of the post-natal development of normal mouse brain by DTI," *Gene*, no. November 2006, pp. 413–421, 2007.

[31] L. A. Harsan, P. Poulet, B. Guignard, N. Parizel, P. L. D. Sousa, N. Boehm, D. Grucker, and M. S. Ghandour, "Brain Dysmyelination and Recovery Assessment by Noninvasive In Vivo Diffusion Tensor Magnetic Resonance Imaging," *Journal of Neuroscience Research*, vol. 402, no. September 2005, pp. 392–402, 2006.

[32] C. Langkammer, N. Krebs, W. Goessler, E. Scheurer, K. Yen, F. Fazekas, and S. Ropele, "Susceptibility induced gray-white matter MRI contrast in the human brain.," *NeuroImage*, vol. 59, no. 2, pp. 1413–9, Jan. 2012.

[33] C. Liu, W. Li, G. A. Johnson, and B. Wu, "High-field (9.4T) MRI of brain dysmyelination by quantitative mapping of magnetic susceptibility.," *NeuroImage*, vol. 56, no. 3, pp. 930–8, Jun. 2011.

[34] I. Bertini, C. Luchinat, and G. Parigi, "Magnetic susceptibility in paramagnetic NMR," *Progress in Nuclear Magnetic Resonance Spectroscopy*, vol. 40, no. 3, pp. 249–273, Apr. 2002.

[35] S. M. Dubiel, B. Zablotna-Rypien, and J. B. Mackey, "Magnetic properties of human liver and brain ferritin.," *European biophysics journal© : EBJ*, vol. 28, no. 3, pp. 263–7, Jan. 1999.

[36] B. Todorich, X. Zhang, and J. R. Connor, "H-ferritin is the major source of iron for oligodendrocytes.," *Glia*, vol. 59, no. 6, pp. 927–35, Jun. 2011.

[37] Stueber, Carsten, Andreas Schaefer, Miriam Waehnert, and J Vogt. "Iron and Myelin in Human Brain Tissue: Histology, PIXE and Ultra-High-Field MRI Susceptibility Maps." *Ww4.aievolution.com* (2012): 23–24. http://ww4.aievolution.com/hbm1201/index.cfm?do=abs.viewAbs&abs=4817.

[37] B. Thomas, S. Somasundaram, K. Thamburaj, C. Kesavadas, A. K. Gupta, N. K. Bodhey, and T. R. Kapilamoorthy, "Clinical applications of susceptibility weighted MR imaging of the brain - a pictorial review.," *Neuroradiology*, vol. 50, no. 2, pp. 105–16, Feb. 2008.

[38] Lodygensky, Gregory a, José P Marques, Rajika Maddage, Elodie Perroud, Stéphane V Sizonenko, Petra S Hüppi, and Rolf Gruetter. "In Vivo Assessment of Myelination by Phase Imaging at High Magnetic Field." *NeuroImage* 59, no. 3 (February 1, 2012): 1979–87. doi:10.1016/j.neuroimage.2011.09.057.

[39] Wharton, S., & Bowtell, R. (2012). “Fiber orientation-dependent white matter contrast in gradient echo MRI.” Proceedings of the National Academy of Sciences.

[40] Basser, Peter J., James Mattiello, and Denis LeBihan. "MR diffusion tensor spectroscopy and imaging." *Biophysical journal* 66, no. 1 (1994): 259-267.